Available online at www.sciencedirect.com
ScienceDirect
Journal of Sound and Vibration 318 (2008) 702–714
JOURNAL OF SOUND AND VIBRATION
www.elsevier.com/locate/jsvi

A geometric approach to the design of remotely located vibration control systems

Steve Daley*, Jiqiang Wang

Department of Automatic Control and Systems Engineering, The University of Sheffield, Mappin Street, Sheffield S1 3JD, UK

Received 17 April 2007; received in revised form 17 April 2008; accepted 21 April 2008
Handling Editor: C.L. Morfey
Available online 10 June 2008

Abstract

Over the past three decades, a wide variety of active control methods have been proposed for controlling problematic vibration. The vast majority of approaches make the implicit assumption that sensors can be located in the region where vibration attenuation is required. For many large scale structures or where the system environment is harsh, this is either not feasible or it is prohibitively expensive. As a result, the optimal control of local vibration may lead to enhancement at remote locations. Motivated by such problems in marine system environments, this paper describes a simple geometric methodology that provides an approach for defining the design freedom available for reducing vibration both at local and remote locations. The results can be used to develop design procedures for both discrete frequency and broad-band control. Robustness to modelling error can also be treated in the same geometric framework. Validation of the approach is carried out using an experimental facility that has been developed to replicate the problems associated with rotor blade vibration.

1. Introduction

Vibration problems generally occur either at specific discrete frequencies, caused by periodic disturbances such as out of balance forces in rotating machines, or in a narrow band, often associated with lightly damped structural modes. For both discrete frequency (or harmonic) and narrow-band control, the design aim is to minimize the vibration at specific *measured* points on a structure and a number of well established design methods are available (for example Refs. [1–5]). The optimum solution is often based solely on information local to the actuators and implementation can, in practice, result in increased levels of vibration at *remote* locations. Such problems are particularly evident in large scale interconnected structures where it is neither feasible nor cost effective to provide a wide distribution of sensors and actuators. Attainment of a globally optimal solution may therefore necessitate the implementation of a locally sub-optimal one.

The work presented here was motivated by the first author's previous research in the area of vibration control for marine systems [6] and where, specifically, it is not practically viable to permanently locate sensors

*Corresponding author. Tel.: +44 114 222 5608; fax: +44 114 222 5661.
E-mail address: steve.daley@sheffield.ac.uk (S. Daley).

0022-460X/$ - see front matter © 2008 Published by Elsevier Ltd.
doi:10.1016/j.jsv.2008.04.050

at all points where vibration attenuation is ultimately required. This is particularly true in ship propulsion transmission systems where propeller blade excitation at specific blade passing frequencies can lead to significant large area hull excitation causing passenger and crew discomfort, self-noise sonar interference and, in extreme cases, catastrophic fatigue failure [7,8]. Similar problems occur in helicopter rotor systems where blade-induced vibration transmits through the fuselage which, not only compromises the reliability of on-board electronic equipment, but also leads to reduced flight envelopes [9]. Also in aerospace applications, the increasing use of lightweight and flexible structures often results in wide area flow-induced vibration that can lead to dynamic aero-elastic instabilities such as wing flutter, with the potential to cause structural failures in flight [10].

Although the issue addressed here is relevant to a wide variety of systems, it is particularly apposite for bladed power transmission systems. The active approach to vibration control of a practical rotor blade system is made particularly difficult by the harsh environment in the proximity of the blades. There are also difficulties relating to the practical implementation of actuators and sensors in rotating frames [11]. Nevertheless, a number of active and semi-active solutions have been proposed to tackle the vibration problem at source by, for example, the integration of smart materials into the blades [12–14]. However, such solutions are costly, difficult to maintain and are unproven in real operational environments. An alternative approach is to attenuate the resultant vibration by actuating within the shafting system [6,15], but this can lead to increased excitation of the blades or elsewhere in the power train. This is tackled here by considering the generic problem of determining strategies for the attenuation of both the local and the remote vibration using only local sensing and control actions.

In the paper a number of new results are presented that define the freedom available to the designer for providing both local and remote vibration reduction and a simple, yet powerful, geometric design methodology is introduced. The efficacy of the new design methodology is illustrated using a laboratory scale test rig that has been developed to replicate the generic problems associated with the propagation of rotor blade vibration through the power train.

2. Geometric controller design

2.1. Preliminaries

It is assumed that the vibrating system can be described by the following frequency response function (FRF):

$$\begin{bmatrix} y(\mathrm{j}\omega) \\ z(\mathrm{j}\omega) \end{bmatrix} = \begin{bmatrix} g_{11}(\mathrm{j}\omega) & g_{12}(\mathrm{j}\omega) \\ g_{21}(\mathrm{j}\omega) & g_{22}(\mathrm{j}\omega) \end{bmatrix} \begin{bmatrix} u(\mathrm{j}\omega) \\ d(\mathrm{j}\omega) \end{bmatrix}, \tag{1}$$

where $y(\mathrm{j}\omega)$, $z(\mathrm{j}\omega)$, $u(\mathrm{j}\omega)$ and $d(\mathrm{j}\omega)$ represent the locally measured vibration, the remote vibration, the control force and the disturbance force respectively. The control aim is to achieve reductions in both $y(\mathrm{j}\omega)$ and $z(\mathrm{j}\omega)$ (where possible) through the application of the feedback control law:

$$u(\mathrm{j}\omega) = -k(\mathrm{j}\omega)y(\mathrm{j}\omega). \tag{2}$$

Although a measurement of $z(\mathrm{j}\omega)$ is not available during implementation, it is assumed that the transfer function matrix:

$$G = \begin{bmatrix} g_{11}(\mathrm{j}\omega) & g_{12}(\mathrm{j}\omega) \\ g_{21}(\mathrm{j}\omega) & g_{22}(\mathrm{j}\omega) \end{bmatrix} \tag{3}$$

can be obtained during a commissioning phase (robustness to modelling error is considered later in Section 2.4 of the paper). It will be noted that the system model, Eq. (1), together with controller, Eq. (2), can be represented by the linear fractional transformation description (Fig. 1) that is commonly used in modern H_∞ and H_2 design procedures [16]. Although such procedures can be useful for discrete frequency and narrow-band control (through a suitable definition of weighting filters), the "handle-turning" nature of the solution means that valuable physical insight into the existence of suitable solutions is often lost.

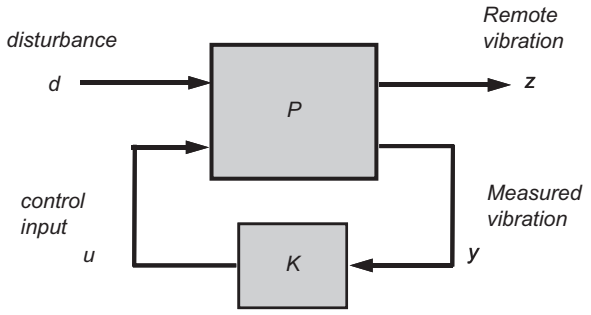

Fig. 1. Linear Fractional Transformation Representation.

By combining Eqs. (1) and (2) to obtain the closed loop transfer functions, $y(j\omega)/d(j\omega)$ and $z(j\omega)/d(j\omega)$, respectively, the problem can be stated as finding the compensator $k(j\omega)$ that simultaneously satisfies:

$$\left|\left(1+g_{11}(j\omega)k(j\omega)\right)^{-1}\right|<1 \tag{4}$$

and

$$\left|1-g_{22}^{-1}(j\omega)g_{21}(j\omega)k(j\omega)(1+g_{11}(j\omega)k(j\omega))^{-1}g_{12}(j\omega)\right|<1, \tag{5}$$

either for a discrete frequency $\omega=\omega_o$ or in the case of broad-band control $\forall\omega\in[\omega_1,\omega_2]$. Satisfying inequality (4) will reduce vibration levels at the locally measured point with respect to the uncontrolled case, whereas satisfying inequality (5) will ensure a relative improvement for the remote location.

The discrete frequency and broad-band cases are treated separately in Sections 2.2 and 2.3, and the robustness to modelling error is considered in Section 2.4.

2.2. Harmonic control

For ease of exposition, the notation does not include an explicit dependency on frequency so within this section the use of g_{11} etc. should be interpreted as $g_{11}(j\omega_o)$. Defining the sensitivity at this discrete frequency by the complex number α, then the closed loop response for y can be expressed as

$$y=\alpha g_{12}d, \tag{6}$$

where for attenuation at this point, $|\alpha|<1$ (a restatement of condition 4). It follows that

$$k=\frac{(1-\alpha)}{\alpha g_{11}}. \tag{7}$$

Condition (5) can therefore be restated as

$$\left|(\alpha-1)\frac{g_{12}g_{21}}{g_{11}g_{22}}+1\right|<1 \tag{8}$$

or with the definition:

$$\beta=(\alpha-1)\frac{g_{12}g_{21}}{g_{11}g_{22}} \tag{9}$$

simply,

$$|\beta+1|<1. \tag{10}$$

Condition (4) can also be expressed as a function of β by rearranging (9) and substituting in $|\alpha|<1$ resulting in

$$\left|\beta\frac{g_{11}g_{22}}{g_{12}g_{21}}+1\right|<1 \tag{11}$$

or

$$|\gamma + 1| < 1 \tag{12}$$

with the definition

$$\gamma = \beta \frac{g_{11} g_{22}}{g_{12} g_{21}} = \beta \tilde{g}. \tag{13}$$

Conditions (10) and (12) are entirely equivalent to (5) and (4) respectively and it will be noted that both describe the equation of a unit circle (and its interior) on the complex plane with centre located at $(-1,0)$. It is possible, therefore, to achieve simultaneous reduction in both $y(j\omega)$ and $z(j\omega)$ for a discrete frequency $\omega = \omega_o$ provided that for a β located within the unit circle with centre $(-1,0)$, there exists a γ satisfying Eq. (12) that is also located within the same circle.

This can be developed further by noting that if the interior of the unit circle with centre $(-1,0)$ on the complex β-plane is mapped onto the complex γ-plane then the result is also a circle (and its interior) with centre at $-\tilde{g}$ and radius $|\tilde{g}|$. It follows therefore that where this circle intersects with the unit circle with centre $(-1,0)$ simultaneous reduction of $y(j\omega)$ and $z(j\omega)$ for a discrete frequency $\omega = \omega_o$ is achievable.

This is illustrated in Fig. 2 from which a number of important results follow directly.

Proposition 1. *Provided that* $|\tilde{g}(j\omega_o)| \neq 0$ *and* $\mathrm{Re}(\tilde{g}(j\omega_o)) > 0$ *if* $\mathrm{Im}(\tilde{g}(j\omega_o)) = 0$ *then a controller* $k(j\omega_o)$ *can always be found to achieve simultaneous reduction in both* $y(j\omega_o)$ *and* $z(j\omega_o)$.

Proposition 2. *The optimal controller* $k_{\mathrm{opt}}(j\omega_o)$ *results from* γ_{opt}, *a point taken from the line on the complex* γ*-plane that joins the point* $(-1,0)$ *with the point* $-\tilde{g}$.

The exact location of γ_{opt} depends upon the control objective. If for example this is to produce maximum attenuation of z without increasing y then, assuming that the point $-\tilde{g}$ is located outside of the unit circle with centre $(-1,0)$, the optimal point is at the intersection of this circle with the line that joins the two centres. If, however, the optimum simultaneous attenuation of both z and y is required, γ_{opt} will be located at the mid-point of the line that joins the two centres. It will also be noted that either end of the optimal line corresponds either to a situation where the controller will provide perfect control of local vibration (i.e. $y = 0$), at point $(-1,0)$ or perfect control of the remote vibration ($z = 0$), at point $-\tilde{g}$. This observation leads to the following results.

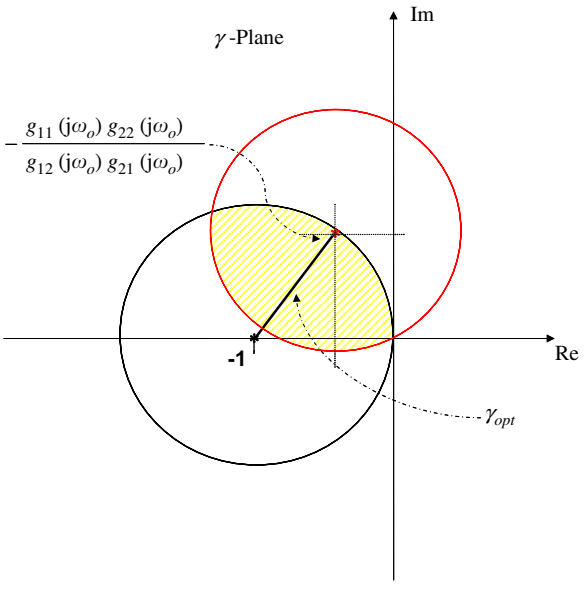

Fig. 2. Mapping of $|\beta + 1| = 1$ on the complex γ-plane.

Proposition 3. *A controller exists that can reduce $z(j\omega_o)$ to zero without leading to an increase in $y(j\omega_o)$ if and only if $\tilde{g}(j\omega_o)$ is positive real and is located on or inside the unit circle having centre at* (1,0) *on the complex plane.*

Proposition 4. *A controller exists that can reduce $y(j\omega_o)$ to zero without leading to an increase in $z(j\omega_o)$ if and only if* $\mathrm{Re}(\tilde{g}(j\omega_o)) \geqslant 0.5$.

It is clear that for the case that $\tilde{g}(j\omega_o)$ is located inside the unit circle having centre at (1,0) and $\mathrm{Re}(\tilde{g}(j\omega_o)) \geqslant 0.5$ the designer will have the choice to reduce either $z(j\omega_o)$ or $y(j\omega_o)$ to zero; further for the special case $\tilde{g}(j\omega_o) = 1$ the same controller will annihilate both. It should be noted, however that since

$$k = -\frac{\gamma}{(1+\gamma)g_{11}}, \tag{14}$$

perfect control of $y(j\omega_o)$ via feedback is impractical in this simple form due to the requirement for infinite gain, although an instantaneous harmonic controller structure [17] can be used.

The results presented here can also be extended to include the case where a specific level of closed-loop attenuation is required by scaling the respective circles accordingly. The case where the requirement is to reduce the vibration levels simultaneously across a range of frequencies is considered in the following section.

2.3. Broad-band control and stability considerations

The case where it is required to reduce $y(j\omega)$ and $z(j\omega)$ $\forall\omega \in [\omega_1,\omega_2]$ can be approached by noting that for every frequency in the range, from Proposition 1, $\gamma(j\omega)$ can be selected to satisfy conditions (10) and (12). However, the distinction from the single discrete frequency case is that for every $\omega \in [\omega_1,\omega_2]$ the mapping of Eq. (10) onto the complex γ-plane results in a separate circle. As a result the optimal solution, $\gamma_{\mathrm{opt}}(j\omega)$, can be represented as a contour on the complex γ-plane, this is illustrated in Fig. 3. Note that for ease of exposition the explicit dependency of the variables on frequency is not included in the notation for the remainder of the section.

Depending on the control objective it then becomes possible to express γ_{opt} as a function of the elements of the transfer function matrix (3). For example, the contour that provides the optimum reduction in z without increasing y can be expressed as

$$\gamma_{\mathrm{opt}} = \begin{cases} -\tilde{g}, & |1-\tilde{g}| \leqslant 1, \\ \gamma_r + j\gamma_i, & |1-\tilde{g}| > 1, \end{cases} \tag{15}$$

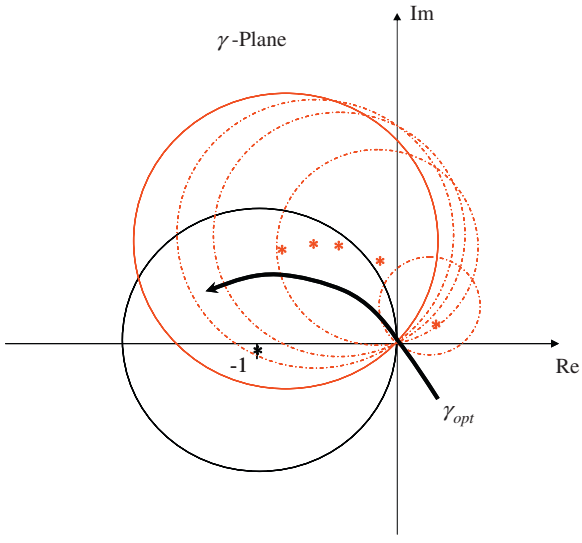

Fig. 3. Mapping of $\gamma_{\mathrm{opt}}(j\omega)$ on the complex γ-plane.

where

$$\gamma_r = \frac{(1 - \mathrm{Re}(\tilde{g}))}{\sqrt{(1 - \mathrm{Re}(\tilde{g}))^2 + \mathrm{Im}(\tilde{g})^2}} - 1,$$
$$\gamma_i = \frac{-\mathrm{Im}(\tilde{g})}{\sqrt{(1 - \mathrm{Re}(\tilde{g}))^2 + \mathrm{Im}(\tilde{g})^2}}. \tag{16}$$

Such a result would appear to imply that a compensator exists that would provide simultaneous reduction (or at least not enhancement) across an arbitrarily wide range of frequencies. Of course this is not necessarily true as there has been no consideration of closed loop stability. The question that needs to be asked therefore is whether it is possible to select γ_{opt} such that the resulting compensator ensures closed loop stability. The answer to this is provided in the following main result:

Proposition 5. *If $g_{11}(\mathrm{j}\omega)$ is both stable and minimum phase and $\gamma_{\mathrm{opt}}(\mathrm{j}\omega)$ is a mapping of a stable function and, in addition, $\mathrm{Re}(\gamma_{\mathrm{opt}}) > -1$ when $\mathrm{Im}(\gamma_{\mathrm{opt}}) = 0$, then the resulting compensator will provide internal closed loop stability.*

The proof follows from noting that the loop gain can be described by

$$L = kg_{11} = \frac{-\gamma}{1 + \gamma}. \tag{17}$$

On inspection of the form of Eq. (17) (i.e. equivalent to a closed loop system with loop gain γ), it is apparent that L will be stable if γ is also stable and its mapping of the Nyquist D-contour does not enclose the $(-1,0)$ point. If L is stable then the closed loop system will also be stable if in addition the mapping of the Nyquist D-contour of L does not enclose the $(-1,0)$ point on the complex plane. It is straightforward to show that both of these stability conditions can simultaneously be met by ensuring that the γ contour always crosses the real axis in the complex γ-plane to the right of the $(-1,0)$ point. If g_{11} is stable and minimum phase, then, for a stable L, k will be stable and there will be no unstable pole-zero cancellations between g_{11} and k. This completes the proof.

The assumption that g_{11} is both stable and minimum phase is not unduly restrictive since given the problem outlined in the introduction, it is very likely that the sensor and actuator can be arranged to be collocated. The requirement for γ to be stable is not as straight forward but could be approached, for example, by fitting an FIR filter (stable by definition) to the γ_{opt} contour. Note that the design can still proceed by using optimum conditions such as given in Eq. (15), but in the region of cross-over the contour must be modified to satisfy $\mathrm{Re}(\gamma_{\mathrm{opt}}) > -1$.

2.4. Robustness to modelling error

Since the above design procedures start from the premise that the frequency response functions are obtained during a calibration process, it is important to consider the effects of model uncertainty on performance. Because of the nature of the implementation, with sensors monitoring only the local vibration, it is logical to consider uncertainty associated with g_{11} separately to that of g_{12}, g_{21} and g_{22}. As a result two multiplicative uncertainty terms are considered as follows:

$$g_{11}^p = g_{11}^o(1 + \Delta_{11}) \tag{18}$$

and

$$\frac{g_{21}^p g_{12}^p}{g_{22}^p} = \frac{g_{21}^o g_{12}^o}{g_{22}^o}(1 + \Delta), \tag{19}$$

where the superscripts "p" and "o" denote the true plant and the nominal design models respectively. With these definitions it can be shown that the reduction of the local vibration in the presence of uncertainty

requires that γ^o, selected on the basis of the nominal model, also satisfies

$$\frac{|1+\gamma^o|}{|1-\gamma^o\Delta_{11}|}<1. \tag{20}$$

The equivalent condition for the reduction of the remote vibration in the presence of the uncertainty is

$$\left|1+\frac{\gamma^o(1+\Delta)}{(1-\gamma^o\Delta_{11})\tilde{g}^o}\right|<1 \tag{21}$$

which follows from the definition of

$$\tilde{g}^o=\frac{g^o_{11}g^o_{22}}{g^o_{12}g^o_{21}} \tag{22}$$

and the combination of the true plant with Eqs. (13) and (10).

Since by definition $|1+\gamma^o|\leqslant 1$, a sufficient condition for (20) to be satisfied is

$$|1-\gamma^o\Delta_{11}|>1. \tag{23}$$

This can also be interpreted geometrically as an increase in the radius of the circle from which γ^o can be selected to still produce a reduction in the local vibration. As a result, if condition (23) is satisfied, the attenuation of local vibration in the face of control path uncertainty will be greater than predicted for the nominal design.

As the sensors and actuators are available at the local position to periodically re-calibrate the system, it is reasonable to assume that $\Delta_{11}=0$ whereupon condition (20) is satisfied by definition and condition (21) reduces to

$$\left|1+\frac{\gamma^o(1+\Delta)}{\tilde{g}^o}\right|<1. \tag{24}$$

This thereby defines the maximum uncertainty that can be tolerated without increasing the remote vibration with the nominal design. For the case that the intention had been to annihilate the remote vibration then $\gamma^o=-\tilde{g}^o$ and condition (24) further simplifies to

$$|\Delta|<1. \tag{25}$$

As a result up to 100% multiplicative uncertainty can be tolerated whilst maintaining simultaneous vibration attenuation and the direct correspondence between uncertainty magnitude and performance loss is clear. It will be noted that condition (24) also has a geometric interpretation and can be considered to be a perturbation of the centre and radius of the nominal mapping of the unit β-circle on the complex γ-plane as illustrated in Fig. 4 (where $\hat{g}=\tilde{g}^o/(1+\Delta)$). Since by definition the perturbation is unknown, then the most robust selection from the nominal optimal line (Fig. 2), is for $\gamma^o=\gamma^o_r+\mathrm{j}\gamma^o_i$ to be selected as the mid-point of its intersection with the unit γ-circle and the mapping of the unit β-circle on the complex γ-plane (denoted by the triangular symbol in Fig. 4). The coordinates of this point are given by

$$\gamma_r=\frac{(1-\mathrm{Re}(\tilde{g}))\left[1+\dfrac{1-|\tilde{g}|}{\sqrt{(1-\mathrm{Re}(\tilde{g}))^2+\mathrm{Im}(\tilde{g})^2}}\right]}{2}-1, \tag{26}$$

$$\gamma_i=\frac{-\mathrm{Im}(\tilde{g})\left[1+\dfrac{1-|\tilde{g}|}{\sqrt{(1-\mathrm{Re}(\tilde{g}))^2+\mathrm{Im}(\tilde{g})^2}}\right]}{2}. \tag{27}$$

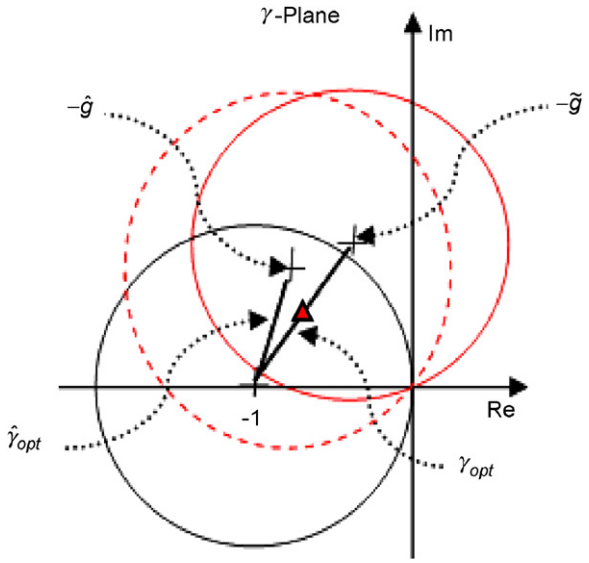

Fig. 4. Mapping of $|\beta+1|=1$ on the complex γ-plane under uncertainty.

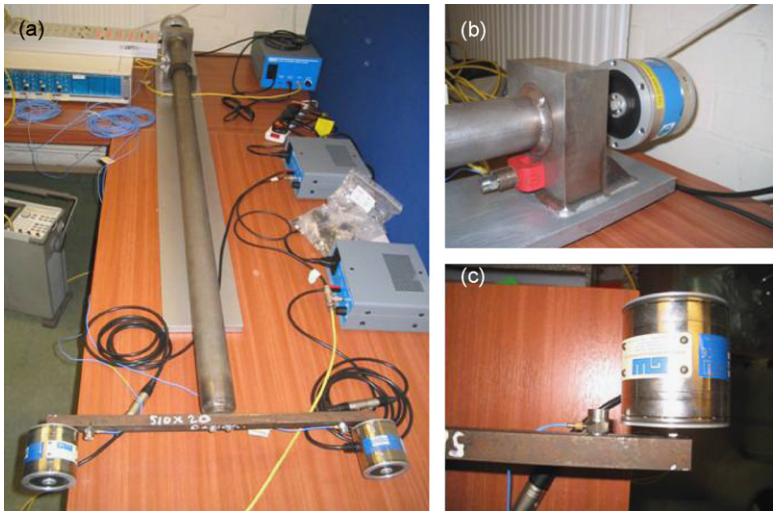

Fig. 5. Blade vibration experimental rig: (a) main view showing beam and hollow shaft, (b) steel block with control shaker and control loop accelerometer and (c) beam with disturbance shaker and monitoring accelerometer.

3. Experimental validation

3.1. Blade vibration facility

The main results of the paper are demonstrated by using them to design a discrete frequency controller for the experimental facility shown in Fig. 5. The facility has been constructed to replicate the key problems associated with the transmission of rotor blade vibration that were discussed in the introduction. The remote control problem arises from the fact that it is desired to control both blade vibration and onward transmission

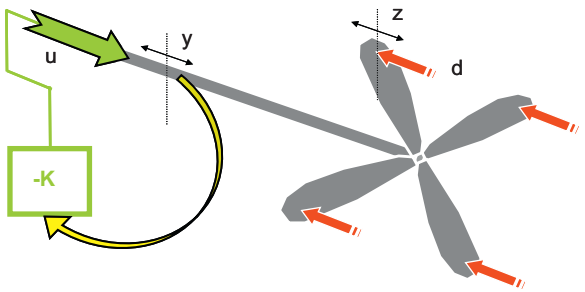

Fig. 6. Remote control of rotor blade vibration.

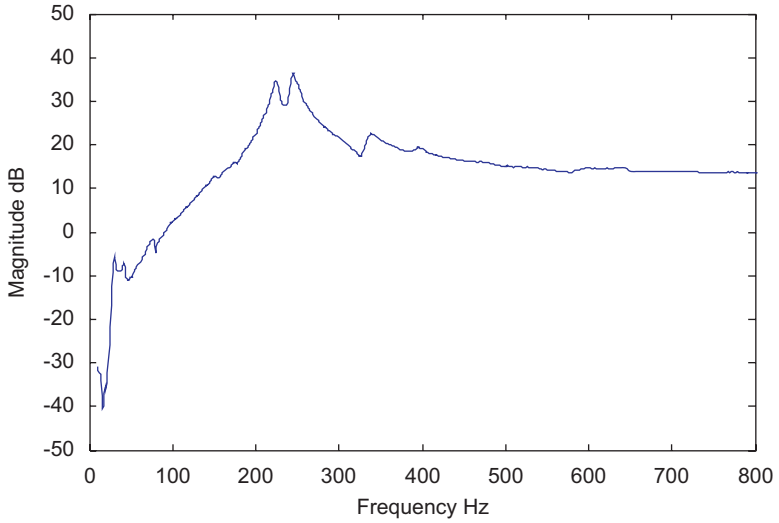

Fig. 7. Magnitude of frequency response function relating the beam acceleration to the beam excitation shakers command signal.

through the power train using only sensors and actuators located at the thrust bearing end of the shaft[1]. This concept is illustrated in Fig. 6 where, in the context of Eq. (1), $y(j\omega)$ represents the axial vibration of the thrust bearing, $z(j\omega)$ the axial vibration of the blades, $u(j\omega)$ the control force applied at the thrust bearing and $d(j\omega)$ the disturbance forces that excite the blades. This does represent a case where during a commissioning phase all the necessary transfer functions can be measured but where it is not currently practically viable to provide in-service sensing and actuation of the blade.

To represent the rotor blade, the test rig has a flexible beam; this is pinned in the centre to one end of a hollow shaft that represents the rotor. The other end of the shaft is fixed to a steel block, representing the thrust bearing, which is rigidly connected to the supporting foundation. The beam can be excited by two small 30 N Gearing and Watson IV40 inertial shakers, to simulate the effect of hydrodynamic or aerodynamic loading on the blades; and at the fixed end of the shaft, a 50 N Gearing and Watson IV45 shaker implements the control force. For monitoring and calibration purposes only, the vibration in the beam is measured by two accelerometers located close to the shakers and another accelerometer used in the control loop measures the acceleration of the block. The controller software is developed in the Matlab/Simulink environment and implemented digitally at a sample rate of 5 kHz using a dSPACE system based upon the Power PC 604e

[1]Note this general concept is the subject of several BAE Systems patents.

processor and Texas Instruments TMS320 DSP. All measurements are conditioned with 8th-order Butterworth anti-aliasing filters with a 700 Hz break frequency.

3.2. Analysis and experimental results

Fig. 7 shows the frequency response of the sum beam acceleration to excitation of the beam using a common force for both shakers (the plot is therefore of $|g_{22}(j\omega)|$). It can be seen that the first bending mode resonance occurs in the region of 244 Hz and that this leads to a peak in the transmission along the shaft, as can be seen in the block response to the same forcing ($|g_{22}(j\omega)|$), Fig. 8.

The problem therefore considered is the extent to which simultaneous reduction in both $y(j\omega_o)$ and $z(j\omega_o)$ can be achieved for $\omega_o = 244$ Hz.

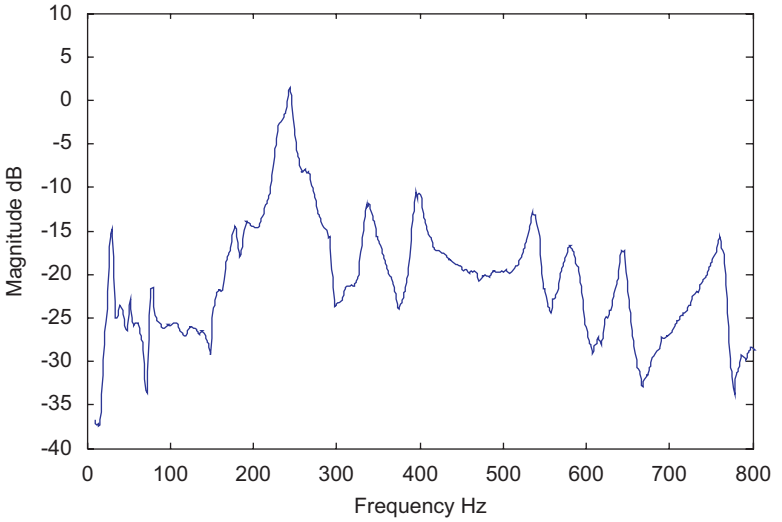

Fig. 8. Magnitude of frequency response function relating the steel block acceleration to the beam excitation shakers command signal.

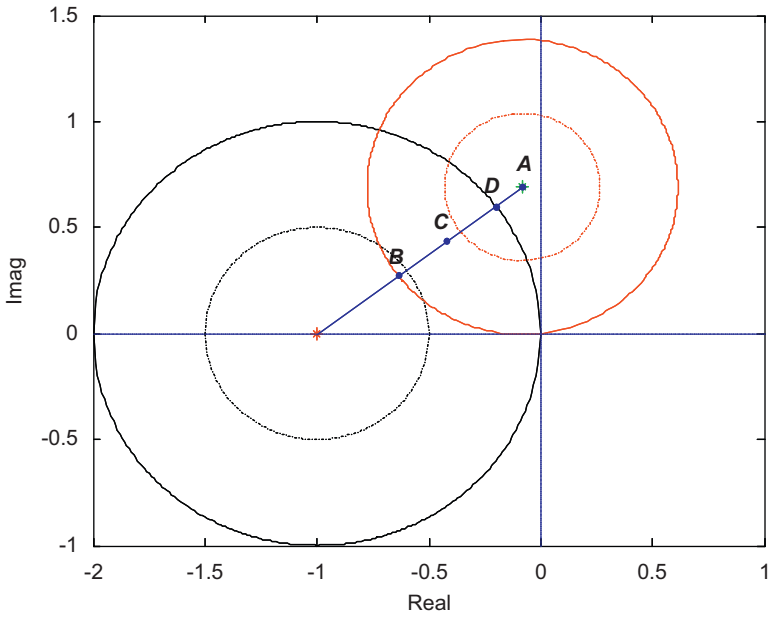

Fig. 9. Mapping of $|\beta + 1| = 1$ on the complex γ-plane for 244 Hz.

The mapping of conditions (10) and (12) onto the complex γ plane for the blade vibration rig measured responses at 244 Hz is shown in Fig. 9. Also shown (dotted circles) are the mappings that represent a 6 dB attenuation boundary for $y(j\omega_o)$ and $z(j\omega_o)$, respectively. It is clear that there is a significant area of intersection where simultaneous reduction of both $y(j\omega_o)$ and $z(j\omega_o)$ is theoretically possible.

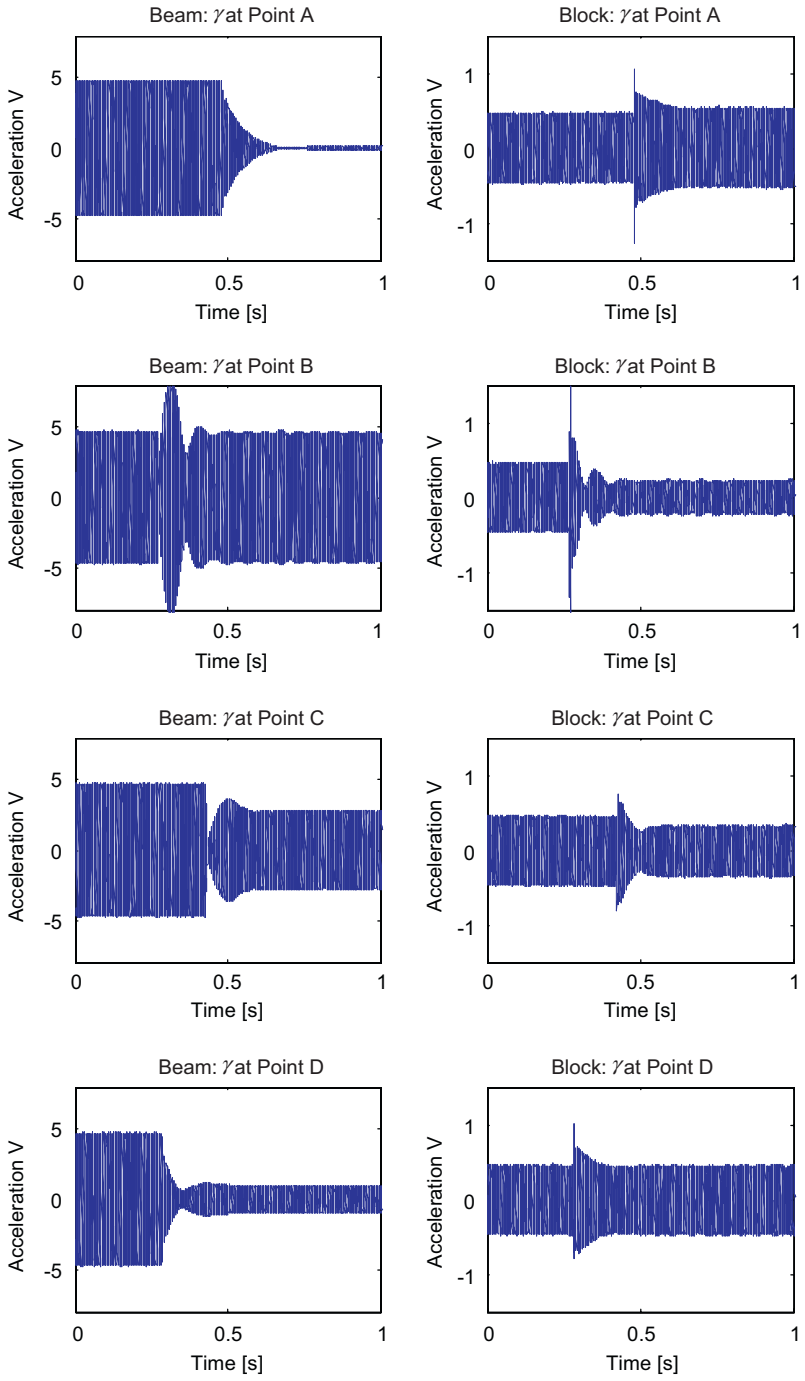

Fig. 10. Acceleration time histories for each of the 244 Hz controllers. The left column displays the sum blade acceleration for each of the controller design points A–D marked in Fig. 9 and the right column displays the corresponding block acceleration.

To illustrate the performance and validate the theory outlined above, four points, labelled A–D in Fig. 9 are selected to construct discrete frequencies controllers (via Eq. (14)). Based on their location on the complex γ plane it is anticipated that the points A–D will respectively, annihilate $z(j\omega_o)$ whilst marginally increasing $y(j\omega_o)$, leave $z(j\omega_o)$ unchanged whilst reducing $y(j\omega_o)$ by a little over 6 dB, reduce $z(j\omega_o)$ by a little under 6 dB whilst reducing $y(j\omega_o)$ by around 3 dB (the mid-point of the region of intersection and most robust selection as defined by Eqs. (26) and (27)) and reduce $z(j\omega_o)$ by around 12 dB without increasing $y(j\omega_o)$. Each of these controllers was applied to the test rig for the condition of fixed amplitude 244 Hz sinusoidal disturbance forces. The results are shown as acceleration time-histories[2] in Fig. 10, where the left column displays the beam sum acceleration and the right, the corresponding block acceleration, for each controller design. The top row of plots corresponds to a controller designed from a value of γ at point A in Fig. 9, the second row is for a controller from γ at point B, the third row is for a controller from γ at point C and the bottom row is for a controller from γ at point D. The instant at which the controller was turned on in each case will be noted by the first disturbance to the signal amplitude. For all cases it is clear that following convergence to the steady state, the performance predictions obtained from the complex γ plane are correct, thereby validating the theoretical results presented in Section 2 above.

4. Conclusions

A novel geometric vibration controller design approach has been presented in this paper. The method is particularly targeted at situations where it is required to apply control at a particular point on a structure but sensors and actuators can only be located at some remote location. The approach results in a straightforward design strategy where the design freedom available for both remote and local vibration is explicitly parameterized. A number of fundamental results have been developed for discrete frequency control and then extended to cover the broad-band case, where an additional design constraint has been defined to ensure closed-loop stability. Robustness to modelling error has been treated in the same geometric framework. The main theoretical results have been validated through their application to the control of vibration in a test rig that has been constructed to replicate the problems associated with rotor blade vibration propagation.

Acknowledgments

The authors are grateful to BAE SYSTEMS MARINE for the provision of the experimental hardware and especially to John Pearson and Roger Harrison for their continued support of this work.

References

[1] P.A. Nelson, S.J. Elliott, *Active Control of Sound*, Academic Press, London, 1992.
[2] J. Shaw, N. Albion, Active control of the helicopter rotor for vibration reduction, *Journal of the American Helicopter Society* 26 (1981) 32–39.
[3] L.A. Sievers, A.H. von Flotow, Comparison and extensions of control methods for narrow band disturbance rejection, *American Society of Mechanical Engineers NCA* 8 (1990) 11–22.
[4] S.J. Elliott, I.M. Stothers, P.A. Nelson, A multiple error LMS algorithm and its application to the active control of sound and vibration, *IEEE Transactions on Acoustics, Speech and Signal Processing* 35 (1987) 1423–1434.
[5] C.R. Fuller, S.J. Elliott, P.A. Nelson, *Active Control of Vibration*, Academic Press, London, 1996.
[6] S. Daley, F.A. Johnson, J.B. Pearson, R. Dixon, Active vibration control for marine applications, *IFAC Journal of Control Engineering Practice* 12 (2004) 465–474.
[7] M.C. Hartnell-Beavis, M.A. Swinbanks, Some recent practical and theoretical developments in noise reduction in ships, *Proceedings of the IMarE Vibration and Noise Conference*, October 1976, pp. 28–38.
[8] P.Y. Tao, S.S. Ge, T.H. Lee, X. Chen, Thruster and vibration control of marine powertrain using a class of feedforward approximators, *Proceedings of the 2006 IEEE International Conference on Control Applications*, Munich, Germany, October 2006, pp. 2589–2594.

[2]Because of the time axis used, the sinusoidal variation in the acceleration signal cannot be seen; however, the change in signal amplitude is clearly displayed.

[9] J.T. Pearson, R.M. Goodall, I. Lyndon, Active control of helicopter vibration, *IEE: Computing and Control Engineering Journal* 5 (1994) 277–284.
[10] D.H. Kim, J.H. Han, I. Lee, Application of fiber optic sensor and piezoelectric actuator to flutter suppression, *Journal of Aircraft* 41 (2004) 409–411.
[11] R.H. Christensen, I.F. Santos, Modal controllability and observability of bladed disks and their dependency on the angular velocity, *Journal of Vibration and Control* 11 (2005) 801–828.
[12] P.C. Chen, I. Chopra, Wind tunnel testing of a smart rotor with individual blade twist control, *Journal of Intelligent Material Systems and Structures* 8 (1997) 414–425.
[13] R.C. Derham, N.W. Hagood, Rotor design using smart materials to actively twist the blades, *Proceedings of American Helicopter Society 52nd Annual Forum*, Washington, DC, June 1996, pp. 1242–1252.
[14] F.K. Straub, H.T. Ngo, V. Anand, D.B. Domzalski, Development of a piezoelectric actuator for trailing edge flap control of full scale rotor blades, *Smart Materials and Structures* 10 (2001) 25–34.
[15] A. Baz, J. Gilheany, P. Steimel, Active vibration control of propeller shafts, *Journal of Sound and Vibration* 136 (1990) 361–372.
[16] J.M. Maciejowski, *Multivariable Feedback Design*, Addison-Wesley, Reading, 1989.
[17] S. Daley, J. Hatonen, K. Tammi, Instantaneous harmonic vibration control of a flexible rotor, *Proceedings of ACTIVE 2006*, Adelaide, Australia, September 2006.